



Determination of absolute orientation-dependent TiN(0 0 1) and TiN(1 1 1) step energies

S. Kodambaka, S.V. Khare, V. Petrova, A. Vailionis, I. Petrov, J.E. Greene*

Department of Materials Science, Frederick Seitz Materials Research Laboratory, University of Illinois, 104 South Goodwin Avenue, Urbana, IL 61801, USA

Abstract

We employ in situ high-temperature (1030–1250 K) scanning tunneling microscopy to measure adatom island coarsening/decay kinetics and temporal fluctuations around the equilibrium shapes of two-dimensional TiN vacancy islands on atomically-smooth (0 0 1) and (1 1 1) TiN terraces. Using inverse Legendre transformations of the equilibrium island shapes, we obtain relative step energies as a function of step orientation within an orientation-independent scale factor λ , the equilibrium chemical potential of the island per unit TiN molecular area. We then use either quantitative island coarsening measurements [in the case of TiN(0 0 1)] or an exact approach for the analysis of shape fluctuations, applicable to highly anisotropic TiN(1 1 1) islands, to determine λ and, hence, absolute orientation-dependent step energies and step stiffnesses.

© 2004 Elsevier Ltd. All rights reserved.

Keywords: Titanium nitride; Surface thermodynamics; Step energies; Surface diffusion; Scanning tunneling microscopy; Ostwald ripening; Epitaxial thin films

1. Introduction

Bi–NaCl-structure TiN is widely used as a hard wear-resistant coating on cutting tools, a diffusion-barrier layer in microelectronic devices, a corrosion-resistant coating on mechanical components, and an abrasion-resistant layer on optics and architectural glass. Since the elastic and diffusion-barrier properties of TiN are highly anisotropic, controlling polycrystalline TiN film texture is important in all of these applications. This fact has spurred interest in modeling the growth of polycrystalline TiN as a function of

deposition conditions [1]. Such a model, however, requires knowledge of surface, step, and nearest-neighbor interaction energies, all as a function of orientation. Recently, considerable progress has been made toward obtaining absolute orientation-dependent step energies and step stiffnesses [2,3] as well as the activation barriers for island coarsening on TiN(0 0 1) and TiN(1 1 1) surfaces [4,5].

The step formation energy β as a function of step orientation φ is a fundamental parameter used to describe crystal surfaces. $\beta(\varphi)$ is the two-dimensional (2D) analog of the surface free energy $\gamma(\varphi)$. Just as $\gamma(\varphi)$ determines the equilibrium shape of bulk crystals, the variation of β with φ determines the equilibrium shape of 2D islands on a terrace. A related property, the step-edge

*Corresponding author.

E-mail address: jegreene@uiuc.edu (J.E. Greene).

stiffness, $\tilde{\beta}(\varphi) \equiv \beta(\varphi) + d^2\beta(\varphi)/d\varphi^2$, is proportional to the island chemical potential [6] and hence controls island coarsening and decay kinetics.

Experimental determination of orientation-dependent step energies is difficult. Methods involving a combination of 2D island equilibrium shape and step fluctuation measurements [7], 3D equilibrium crystal shape and surface energy [8], temperature-dependence of 2D island equilibrium shapes [9,10], and anisotropic island shape fluctuations [3] have been used to determine absolute step energies. *Orientation-averaged* step energies have been determined from near-isotropic island shape fluctuations [11] and 2D island coarsening measurements [12,13]. However, methods described in Refs. [12,13] alone are not applicable to determine absolute orientation-dependent step energies for anisotropic island shapes.

Here, we present two approaches, both of which are based upon analyses of the 2D equilibrium island shape, for the determination of absolute $\beta(\varphi)$ values on atomically-smooth (001) and (111) TiN terraces using in situ high-temperature scanning tunneling microscopy (STM). The first method employs quantitative STM measurements of island coarsening/decay (Ostwald ripening) kinetics in combination with a modified expression for the Gibbs–Thomson relation describing anisotropic islands. The second method relies on an exact theory for the analysis of shape fluctuations, applicable to highly anisotropic islands. We derive an analytical expression for the orientation dependence of $\beta(\varphi)$ from the equilibrium shape using the inverse Legendre transformation procedure described in Ref. [14]. This provides relative $\beta(\varphi)$ values within an orientation-independent scale factor λ , the equilibrium island chemical potential per unit TiN molecular area, while eliminating the conventional inverse Wulff-construction which involves the tedious procedure of tangent constructions. Next, we analyze quantitative measurements of TiN(001) island coarsening/decay kinetics and TiN(111) island shape-fluctuations and apply the two above-mentioned techniques, respectively to determine λ and, hence, absolute orientation-dependent step energies and step stiffnesses.

2. Experimental

Epitaxial TiN(001) and TiN(111) layers, 2000–3000 Å thick, were grown on MgO(001) and Al₂O₃(11 $\bar{2}$ 0), respectively, by ultra-high vacuum (UHV) magnetically-unbalanced DC magnetron sputter deposition [15] using the procedure described in Refs. [3,4]. The samples were then transferred to a UHV multi-chamber variable-temperature Omicron STM with a base pressure of 2×10^{-10} Torr. The system is equipped with facilities for electron-beam evaporation, ion etching, Auger electron spectroscopy, and low-energy electron diffraction (LEED). Sample temperatures were measured by optical pyrometry and calibrated using temperature-dependent TiN emissivity data obtained by spectroscopic ellipsometry. The TiN layers were degassed in UHV at 1073 K, where the vapor pressure of N₂ over TiN is less than 10^{-10} Torr [16], for approximately 1200 s. Epitaxial TiN(001) or TiN(111) buffer layers, 50–100 Å thick, were deposited at 1023 K by reactive evaporation from Ti rods in 1×10^{-7} Torr N₂ and annealed in N₂ for 4 h at $T_a \approx 1100$ K. This process yields sharp 1×1 LEED patterns corresponding to bulk-terminated surfaces with interplanar spacings of 2.1 Å for TiN(001) and 2.4 Å for TiN(111).

TiN partial monolayers with coverages of up to 0.8 ML were deposited on the TiN buffer layers by reactive-evaporation at room temperature. The partial monolayer samples were annealed in N₂ at $T_a = 1023$ – 1223 K while scanning the surface in the STM. This procedure results in the formation of equilibrium-shaped 2D square TiN islands on (001) terraces and truncated-hexagon islands bounded by $\langle 110 \rangle$ steps on $\langle 111 \rangle$ terraces [3]. We obtain 2D adatom islands at coverages < 0.4 ML and vacancy islands at higher coverages. The TiN(001) islands are single-atom-height while the TiN(111) islands are bilayer-height.¹

For each of the measurement sequences, island boundaries and areas A were determined from the STM images using Image SXM, an image proces-

¹The [111] direction in B1–NaCl structure TiN is polar, consisting of alternating layers of Ti and N atoms.

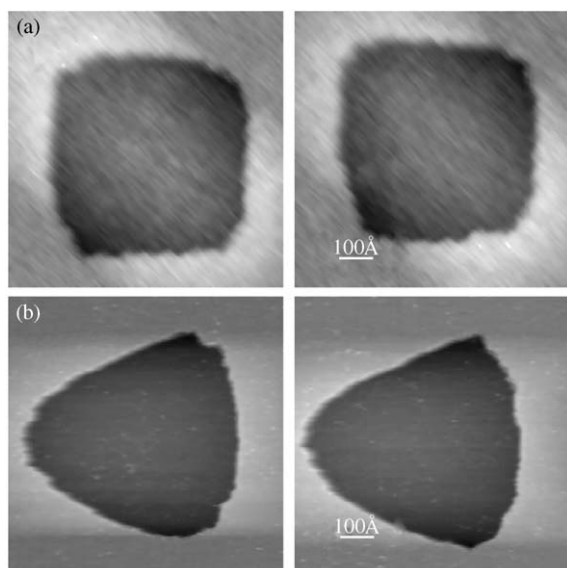


Fig. 1. (a) and (b): Consecutive STM images of 2D TiN vacancy islands on atomically-smooth (001) and (111) TiN terraces, respectively. Image size, scan rate, and annealing temperature T_a : (a) $338 \times 338 \text{ \AA}^2$, 15 s/frame, and 1140 K; (b) $430 \times 430 \text{ \AA}^2$, 32 s/frame, and 1200 K.

sing software.² To determine the equilibrium island shape, we require islands of constant area. Thus, the boundary coordinates $r(\theta, t_a)$ of measured islands, of average radii $> 100 \text{ \AA}$, were normalized to the smallest island area in the measurement sequence following the procedure used in Refs. [2,3]. The equilibrium island shape $R(\theta)$ was then obtained by averaging $r(\theta, t_a)$ at all t_a values within the measurement sequence [2].

3. Results and discussion

3.1. Equilibrium island shape analyses

Fig. 1 consists of two sets of consecutive STM images of 2D TiN vacancy islands on atomically-smooth (001) (Fig. 1a) and (111) (Fig. 1b) TiN terraces acquired at 1140 and 1200 K, respectively. The observed fluctuations in island shapes $r(\theta, t_a)$

²Image SXM, developed by Prof. Steve Barrett, Liverpool, UK; <http://reg.ssci.liv.ac.uk>.

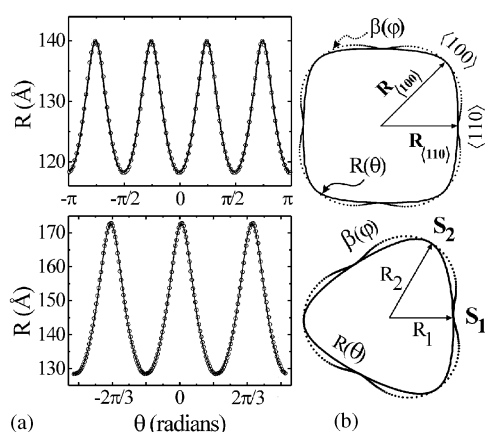


Fig. 2. Upper panel: (a) Plot of R vs. θ for the TiN(001) island shown in Fig. 1a. (b) Polar plot of R vs. θ and β vs. φ determined using Eq. (2) with $\lambda = 1$. Lower panel: The corresponding plots for the TiN(111) island in Fig. 1b. Open circles represent experimental data and the solid lines are the analytical fits obtained using Eq. (1).

are due to thermally induced random motion of the diffusing species.

Equilibrium island shapes $R(\theta)$, determined, using the procedure described above, from the average of all images (typically 15–60) in a given measurement sequence were fit with Lorentzian functions³ of general form,

$$R = R_0 + \frac{a}{[1 + b(\theta - \theta_c)^2]}, \quad (1)$$

where R_0 , a , b , and θ_c are fitting parameters. R vs. θ for the TiN(001) and TiN(111) islands corresponding to Figs. 1a and b are plotted in the upper and lower panels of Fig. 2a.

The open circles represent the measured data while the solid lines are the analytical fits obtained using Eq. (1). All experimental data were equally well fit. The inverse Legendre transform of $R(\theta)$ yields relative values of $\beta(\varphi)$ through the analytical

³Measured $R(\theta)$ data at θ values over the range $0 - \theta_{\text{sym}}$ [with $\theta_{\text{sym}} = \pi/2$ and $2\pi/3$ for TiN(001) and TiN(111), respectively] were fit with two Lorentzian functions. The same set of functions, with θ_c shifted by $n\theta_{\text{sym}}$, $n = 1, 2$, and 3 for TiN(001) and 1 and 2 for TiN(111), were used to fit the data at higher θ values. The form of Eq. (1), which provides an analytical means to calculate \dot{R} and \ddot{R} , has no physical significance.

expression [14]

$$\beta(\varphi) = \lambda \frac{[R(\theta)]^2}{\sqrt{[R(\theta)]^2 + [\dot{R}(\theta)]^2}} \quad (2)$$

with $\varphi = \theta - \arctan(\dot{R}/R)$. \dot{R} in Eq. (2) is the first spatial derivative of R with respect to θ . Polar plots of $\beta(\varphi)$ (dotted line) calculated with $\lambda = 1$ for TiN(001) and TiN(111) islands in Figs. 1a and b are shown in the upper and lower panels, respectively of Fig. 2b. The straight and corner steps are $\langle 110 \rangle$ and $\langle 100 \rangle$, respectively for TiN(001), and are $\langle 110 \rangle$ steps, labeled S_1 and S_2 , for TiN(111).

In order to obtain absolute $\beta(\varphi)$ values, λ in Eq. (2) has to be determined independently. We do this using island coarsening/decay (Ostwald ripening) experiments for TiN(001) and shape-fluctuation measurements for TiN(111) as described below.

3.2. TiN(001) island decay analyses

Ostwald ripening is a phenomenon in which larger islands grow at the expense of smaller ones and is described by the Gibbs–Thomson equation [6,17]

$$\rho^{\text{eq}} = \rho_{\infty}^{\text{eq}} \exp\left(\frac{\beta\Omega}{\tilde{r}kT_a}\right), \quad (3)$$

where ρ^{eq} is the equilibrium free adatom concentration associated with an island of radius \tilde{r} , $\rho_{\infty}^{\text{eq}}$ is the equilibrium free adatom concentration associated with a straight step, and Ω is the unit TiN molecular area. Note that Eq. (3), while commonly used in the literature to represent the Gibbs–Thomson equation, is specific to the case of isotropic (circular) islands. The general equation for anisotropic (non-circular) equilibrium island shapes is

$$\rho^{\text{eq}} = \rho_{\infty}^{\text{eq}} \exp\left(\frac{\tilde{\beta}(\varphi)\kappa(\theta)\Omega}{kT_a}\right). \quad (4)$$

$\kappa(\theta)$ in Eq. (4) is the curvature of the equilibrium island shape given by the relation

$$\kappa(\theta) = \frac{S(\theta)}{R_{\text{avg}}}, \quad (5a)$$

where

$$S(\theta) = \frac{\{[R/R_{\text{avg}}]^2 + 2[\dot{R}/R_{\text{avg}}]^2 - [R\ddot{R}/R_{\text{avg}}^2]\}}{\{[R/R_{\text{avg}}]^2 + [\dot{R}/R_{\text{avg}}]^2\}^{3/2}} \quad (5b)$$

is a dimensionless orientation-dependent curvature function describing the equilibrium shape and $R_{\text{avg}} = \sqrt{A/\pi}$ is the average island radius. \ddot{R} in Eq. (5b) denotes the second spatial derivative of R with respect to θ . The step-edge stiffness $\tilde{\beta}(\varphi)$ is related to $\kappa(\theta)$ through the expression [6,18]

$$\tilde{\beta}(\varphi) = \frac{\lambda}{\kappa(\theta)}. \quad (6)$$

λ , the equilibrium chemical potential of the island per unit TiN molecular area, in Eq. (6), is independent of step orientation and depends only on island size. Thus, by combining Eqs. (5) and (6), we obtain an exact expression for λ in terms of the *orientation-independent* parameters R_{avg} and B :

$$\lambda = \frac{B}{R_{\text{avg}}}, \quad (7a)$$

with

$$B \equiv \tilde{\beta}(\varphi)S(\theta). \quad (7b)$$

B , defined in Eq. (7b), determines the energy scale of the surface equilibrium chemical potential. For the case of circular islands, $B = \beta$ and $R_{\text{avg}} = \tilde{r}$, and we recover Eq. (3). For the case of anisotropic equilibrium island shapes, Eq. (4) can be written in terms of B and R_{avg} , as

$$\rho^{\text{eq}} = \rho_{\infty}^{\text{eq}} \exp\left(\frac{B\Omega}{R_{\text{avg}}kT_a}\right). \quad (8)$$

We have used in situ high-temperature STM to follow 2D adatom island coarsening kinetics on TiN(001) surfaces, where the rate-limiting mechanism is surface diffusion [4], and Eq. (8) to model the results in order to obtain B and, hence, λ . To extract B from time- and temperature-dependent STM measurements, we have chosen a simple experimental geometry, an adatom island in a vacancy pit, where the equilibrium free adatom concentrations around the island are well defined. The decay rate dA/dt_a of an island in this

geometry is given by [4]

$$\frac{dA}{dt_a} = -2\pi\Omega C\rho_\infty^{\text{eq}} \left[\exp\left(\frac{B\Omega}{R_{\text{avg}}kT_a}\right) - \exp\left(\frac{-B\Omega}{R_p kT_a}\right) \right], \quad (9)$$

where the proportionality constant C is a temperature-dependent rate coefficient and R_p is the average radius of the vacancy pit.

We model diffusion-limited island decay kinetics for this configuration using an adaptive iterative finite-element methods to solve the 2D diffusion equation $\partial\rho(x,y)/\partial t = -C\nabla^2\rho(x,y)$ at steady-state [4] with Eq. (8) as a boundary condition. $\rho(x,y)$ is the local adatom concentration and C , for diffusion-limited kinetics, is the surface diffusivity. In the decay curves, the product $C\rho_\infty^{\text{eq}}(T_a)$ determines the time over which an island decays and B defines the shape of the decay curve at small island sizes [12]. It is important to note that the only two unknown parameters in the calculation, B and the product $C\rho_\infty^{\text{eq}}(T_a)$, can be determined accurately from island coarsening measurements *only* when the argument of the exponential, $\exp(B\Omega/R_{\text{avg}}kT_a)$, in Eq. (9) is such that $(B\Omega/R_{\text{avg}}kT_a) \gg 1$. For $(B\Omega/R_{\text{avg}}kT_a) \ll 1$, the exponential can be expanded to first order which yields the mean-field expression where $BC\rho_\infty^{\text{eq}}(T_a)$ is a single parameter. Experimental data, at seven different annealing temperatures, $T_a = 1023$ – 1223 K, for islands that satisfy the condition $(B\Omega/R_{\text{avg}}kT_a) \gg 1$, were fitted with calculated results to determine B and $C\rho_\infty^{\text{eq}}(T_a)$.

Fig. 3 shows a typical plot of measured (open squares) and calculated (solid line) island area A as a function of annealing time t_a , in this case for a 40 \AA adatom island at $T_a = 1140$ K. Decay curves for 14 different adatom islands were equally well fit with $B = 0.23 \pm 0.05 \text{ eV/\AA}$. Combining this result with the measured equilibrium shape in Fig. 2a, we obtain, using Eq. (7), size-dependent λ values.

3.3. Island shape-fluctuation analyses

An alternate approach to determine λ , and hence $\beta(\varphi)$, is based upon the recently-developed

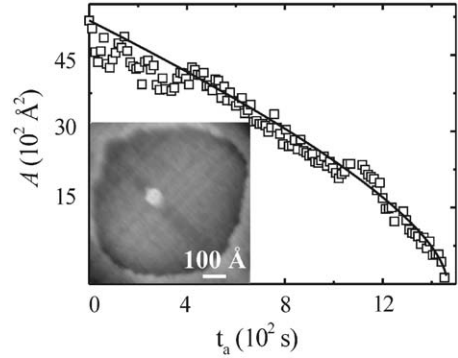


Fig. 3. Measured (open squares) island areas A vs. annealing time t_a for a 2D TiN(001) adatom island in a vacancy pit during annealing at 1140 K. The solid line is the calculated curve obtained using diffusion-limited model with $B = 0.23 \text{ eV/\AA}$. An STM image ($705 \times 715 \text{ \AA}^2$) of the island geometry is given in the inset.

theory of anisotropic island shape-fluctuations. [3,14]. In this section, we apply this method and analyze STM measurements of temporal fluctuations in TiN(1 1 1) island shapes.

The total free energy F of an island is related to the island shape r through the relationship

$$F = \int_0^{2\pi} \{\beta[\varphi(\theta, t_a)](r^2 + \dot{r}^2)^{1/2}\} d\theta. \quad (10)$$

The angle $\varphi(\theta, t_a)$ in Eq. (10) is the local normal to the fluctuating shape at $r(\theta, t_a)$ in contrast to Eq. (2) where φ corresponds to the local normal to the equilibrium shape at $R(\theta)$. Thus, $\beta(\varphi)$ in Eq. (10) is also a function of r and hence t_a . Since the equilibrium shape corresponds to the minimum free energy F_o , temporal deviations $g(\theta, t_a)$ from the equilibrium shape result in a change in free energy $\Delta F \equiv F - F_o$, where we have defined $g \equiv g(\theta, t_a)$ to be the normalized deviation of the temporal shape r from the equilibrium shape R . Thus, $g \equiv [r - R]/R$. In order to derive an expression for λ in terms of the measurable quantity g , we construct a function $f \equiv f(\theta, r, \dot{r})$ defined as

$$f(\theta, r, \dot{r}) = \beta[\varphi(t_a)](r^2 + \dot{r}^2)^{1/2} - \lambda(r^2/2). \quad (11)$$

Note that the second term in Eq. (11) accounts for the constant area constraint with a Lagrange multiplier λ . Expanding f to second order by Taylor's theorem for functions of two variables

(r and \dot{r}) and substituting for $\beta(\varphi)$ from Eq. (2), we derive an expression for ΔF in terms of λ and g ,

$$\Delta F = \frac{\lambda}{2} \left(\int_0^{2\pi} [\chi(\theta, t_a)]^2 d\theta - \int_0^{2\pi} [\rho(\theta, t_a)]^2 d\theta \right), \quad (12)$$

where we define $\chi(\theta, t_a)$ and $\rho(\theta, t_a)$ as

$$\begin{aligned} \chi(\theta, t_a) &\equiv R^2 \dot{g} / (R^2 + 2\dot{R}^2 - R\ddot{R})^{1/2} \\ \rho(\theta, t_a) &\equiv gR. \end{aligned} \quad (13)$$

In Eq. (13), \ddot{R} denotes the second derivative of R with respect to θ . Rewriting the functions as Fourier series $\chi(\theta, t_a) = \sum_n \chi_n(t_a) e^{in\theta}$ and $\rho(\theta, t_a) = \sum_n \rho_n(t_a) e^{in\theta}$ allows Eq. (12) to be expressed in terms of the Fourier components χ_n and ρ_n as $\Delta F = \pi\lambda \sum_n G_n$ in which $G_n = |\chi_n(t_a)|^2 - |\rho_n(t_a)|^2$. Since temporal changes in the total free energy are only due to g , ΔF can be expressed as a homogeneous second-order function in $\{g_n\}$, where $g_n \equiv (1/2\pi) \int_0^{2\pi} g e^{-in\theta} d\theta$. Then, by Euler's theorem, we obtain $\sum_n g_n (\partial \Delta F / \partial g_n) = 2\Delta F$. Comparing the above relation to the generalized equipartition theorem [19], we find that the time-averaged free energy $\langle \Delta F \rangle$ is equal to $N_{\max} k_B T / 2$ where N_{\max} corresponds to the maximum number of allowable fluctuation modes.⁴ Thus, we obtain λ as

$$\lambda = \frac{N_{\max} k_B T}{2\pi \sum_n \langle G_n \rangle}. \quad (14)$$

We have measured the temporal fluctuations of 14 vacancy islands of average radii 50–260 Å over the temperature range $T_a = 1165$ –1248 K. For each island, the equilibrium shape R and g were determined from the STM data. $\chi(\theta, t_a)$ and $\rho(\theta, t_a)$ values were calculated numerically based upon Eq. (13) using the analytical fits to $R(\theta)$ of Eq. (1). The calculated Fourier components G_n were then used in Eq. (14) in order to obtain λ values for all islands.

⁴With the smallest mode corresponding to two surface-atom spacing, N_{\max} is defined as one half of the total number of atoms along the island periphery of a single atomic layer.

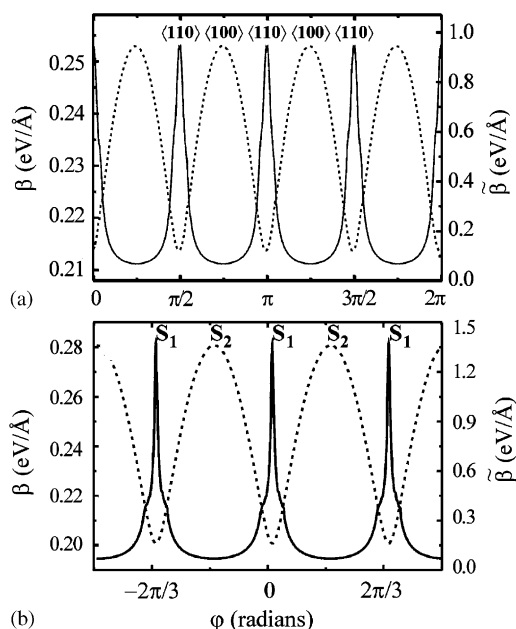


Fig. 4. Absolute values of β vs. φ (dashed line) and $\tilde{\beta}$ vs. φ (solid line) for the (a) TiN(001) island in Fig. 1a and (b) a TiN(111) vacancy island at $T_a = 1248$ K.

3.4. Absolute step energies

Substituting the size-dependent λ values, determined using the procedures described in Sections 3.2 and 3.3, into Eq. (2), we then determine absolute $\beta(\varphi)$ values for TiN(001) and TiN(111). $\kappa(\theta)$ values were calculated for the islands using the $R(\theta)$ fit obtained from Eq. (1). This yields, from Eq. (6), absolute values for $\tilde{\beta}(\varphi)$. Both β (dashed line) and $\tilde{\beta}$ (solid line) for TiN(001) and TiN(111) are plotted as a function of φ in Figs. 4a and b, respectively.

In case of TiN(001), for the two high-symmetry $\langle 110 \rangle$ and $\langle 100 \rangle$ steps we obtain: $\beta_{110} = 0.21 \pm 0.05$, $\tilde{\beta}_{110} = 0.9 \pm 0.2$, $\beta_{100} = 0.25 \pm 0.05$, and $\tilde{\beta}_{100} = 0.07 \pm 0.02$ eV/Å. Averaging over all TiN(111) vacancy islands at all annealing temperatures (1165–1248 K), we obtain step energies β_1 and β_2 for the two $\langle 110 \rangle$ steps of 0.24 ± 0.05 and 0.34 ± 0.08 eV/Å, respectively with step stiffnesses $\tilde{\beta}_1 = 1.6 \pm 0.5$ eV/Å and $\tilde{\beta}_2 = 0.08 \pm 0.01$ eV/Å. The larger uncertainties in determining $\tilde{\beta}_{110}$ and $\tilde{\beta}_1$ values arise from the difficulty in determining the curvature of nearly straight steps.

4. Conclusions

In conclusion, we have shown that measurements of 2D island decay kinetics or shape-fluctuations in combination with analyses of equilibrium island shapes can be used to determine absolute orientation-dependent step energies on anisotropic, as well as, isotropic surfaces. We employed in situ high-temperature (1030–1250 K) STM to measure adatom island coarsening/decay and temporal fluctuations around the equilibrium shapes of two-dimensional TiN vacancy islands on atomically smooth (001) and (111) TiN terraces. Inverse Legendre transformations of the equilibrium island shapes yields relative step energies as a function of step orientation within an orientation-independent scale factor λ , the equilibrium chemical potential of the island per unit TiN molecular area. We then use either quantitative island coarsening measurements [in the case of TiN(001)] or an exact approach for the analysis of shape fluctuations, applicable to highly anisotropic TiN(111) islands, to determine λ and, hence, absolute orientation-dependent step energies and step stiffnesses.

Acknowledgements

The authors gratefully acknowledge the financial support of the U.S. Department of Energy (DOE), Division of Materials Science, under Contract No. DEFG02-91ER45439 through the University of Illinois Frederick Seitz Materials Research Laboratory (FS-MRL). SVK is supported by NSF under Contract No. DMR97-03906. We also appreciate the use of the facilities in the Center for Microanalysis of Materials, partially supported by DOE, at the FS-MRL.

References

- [1] Baumann FH, Chopp DL, de la Rubia TD, Gilmer GH, Greene JE, Huang H, Kodambaka S, O'Sullivan P, Petrov I. *MRS Bull* 2001;26:182–9.
- [2] Kodambaka S, Khare SV, Petrova V, Vailionis A, Petrov I, Greene JE. *Surf Sci* 2002;513:468–74.
- [3] Kodambaka S, Petrova V, Khare SV, Johnson DD, Petrov I, Greene JE. *Phys Rev Lett* 2002;88:146101; Kodambaka S, Khare SV, Petrova V, Johnson DD, Petrov I, Greene JE. *Phys Rev B* 2003;67:035409.
- [4] Kodambaka S, Petrova V, Vailionis A, Petrov I, Greene JE. *Surf Sci* 2003;526:85–96.
- [5] Kodambaka S, Petrova V, Khare SV, Gall D, Rockett A, Petrov I, Greene JE. *Phys Rev Lett* 2002;89:176102.
- [6] Mullins WW. *Interface Sci* 2001;9:9–20.
- [7] Bartelt NC, Tromp RM, Williams ED. *Phys Rev Lett* 1994;73:1656–9.
- [8] Arenhold K, Surnev S, Bonzel HP, Wynblatt P. *Surf Sci* 1999;424:271–7; Bonzel HP, Emundts A. *Phys Rev Lett* 2000;84:5804–7.
- [9] Icking-Konert GS, Giesen M, Ibach H. *Phys Rev Lett* 1999;83:3880–3; Giesen M, Steimer C, Ibach H. *Surf Sci* 2001;471:80–100.
- [10] Emundts A, Nowicki M, Bonzel HP. *Surf Sci* 2002;496: L35–42; Nowicki M, Bombis C, Emundts A, Bonzel HP. *Phys Rev B* 2003;67:075405.
- [11] Schlöber DC, Verheij LK, Rosenfeld G, Comsa G. *Phys Rev Lett* 1999;82:3843–6; Steimer C, Giesen M, Verheij L, Ibach H. *Phys Rev B* 2001;64:085416.
- [12] Morgenstern K, Rosenfeld G, Comsa G. *Phys Rev Lett* 1996;76:2113–6; Morgenstern K, Rosenfeld G, Lægsgaard E, Besenbacher F, Comsa G. *Phys Rev Lett* 1998;80:556–9.
- [13] Schulze Icking-Konert G, Geisen M, Ibach H. *Surf Sci* 1998;398:37–48.
- [14] Khare SV, Kodambaka S, Johnson DD, Petrov I, Greene JE. *Surf Sci* 2003;522:75–83.
- [15] Greene JE, Sundgren JE, Hultman L, Petrov I, Bergstrom DB. *Appl Phys Lett* 1995;67:2928–30.
- [16] Zeng K, Schmid-Fetzer R. *Z Metallkd* 1996;87:540–54.
- [17] Herring C. *The physics of powder metallurgy*. New York: McGraw-Hill; 1951. p. 143.
- [18] Khare SV, Einstein TL. *Phys Rev B* 1996;54:11752–61.
- [19] Huang K. *Statistical mechanics*. New York: Wiley; 1963. p. 149.